

Accepted Manuscript

Four novel coordination frameworks with high degree of diamondoid interpenetration containing scarce quadruple-stranded homo-axis helices and quintuple-stranded molecular braids

Yu Chen, Xi-Chi Wang, Qi Yang, Yu-Ci Xu, Jin-Tao Tong, Hao Yuan, Dong-Rong Xiao

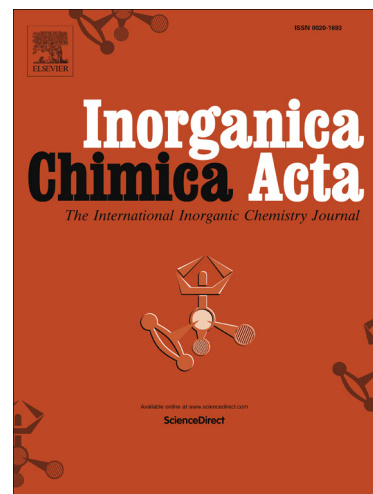
PII: S0020-1693(16)30179-7
DOI: <http://dx.doi.org/10.1016/j.ica.2016.04.018>
Reference: ICA 17002

To appear in: *Inorganica Chimica Acta*

Received Date: 2 March 2016
Revised Date: 7 April 2016
Accepted Date: 10 April 2016

Please cite this article as: Y. Chen, X-C. Wang, Q. Yang, Y-C. Xu, J-T. Tong, H. Yuan, D-R. Xiao, Four novel coordination frameworks with high degree of diamondoid interpenetration containing scarce quadruple-stranded homo-axis helices and quintuple-stranded molecular braids, *Inorganica Chimica Acta* (2016), doi: <http://dx.doi.org/10.1016/j.ica.2016.04.018>

This is a PDF file of an unedited manuscript that has been accepted for publication. As a service to our customers we are providing this early version of the manuscript. The manuscript will undergo copyediting, typesetting, and review of the resulting proof before it is published in its final form. Please note that during the production process errors may be discovered which could affect the content, and all legal disclaimers that apply to the journal pertain.



**Four novel coordination frameworks with high degree of
diamondoid interpenetration containing scarce
quadruple-stranded homo-axis helices and quintuple-stranded
molecular braids**

Yu Chen,^a Xi-Chi Wang,^a Qi-Yang,^a Yu-Ci Xu,^a Jin-Tao Tong,^a Hao Yuan^a and

Dong-Rong Xiao^{*a,b}

^a *College of Chemistry and Chemical Engineering, Southwest University, Chongqing, 400715, PR China. E-mail: xiaodr98@swu.edu.cn*

^b *State Key Laboratory of Structural Chemistry, Fujian Institute of Research on the Structure of Matter, Chinese Academy of Sciences, Fuzhou, Fujian 350002, PR China*

*Corresponding author. Tel: +86-23-68252360; fax: +86-23-68254000.

E-mail address: xiaodr98@swu.edu.cn (D. R. Xiao)

Abstract: Four novel interpenetrated diamondoid (**dia**) networks, namely [Zn(1,4-bdc)(bibp)] (**1**), [Mn(bqdc)(bibp)] (**2**), [Cd(bqdc)(bibp)] (**3**), [Co₄(bqdc)₄(bibp)₄] (**4**). (bibp = 1,4-bis(4-(imidazole-1-yl)benzyl)piperazine, 1,4-bdc = 1,4-benzenedicarboxylate, bqdc = 2,2'-biquinoline-4,4'-dicarboxylate), have been synthesized by using mixed spacer ligands with significantly different lengths. Their structures were determined by single-crystal X-ray diffraction analyses and further characterized by elemental analyses, IR spectra and TG analyses. Compound **1** is an unusual 8-fold [4+4] interpenetrated **dia** network containing the unique quadruple-stranded braid (i.e. quadruple-stranded homo-axis helices), which is further entangled by another quadruple-stranded braid to produce an unprecedented octuple-stranded braid derived from eight individual **dia** nets. Compounds **2** and **3** are isostructural, while compound **4** is isorecticular to them. They all exhibit 5-fold interpenetrating **dia** networks containing an exceptional quintuple-stranded molecular braid. In addition, the photoluminescence properties of compounds **1** and **3**, and the magnetic property of compound **4** were studied.

Keywords: Coordination polymers; Interpenetration; Molecular braid; N ligand; Topology

Introduction

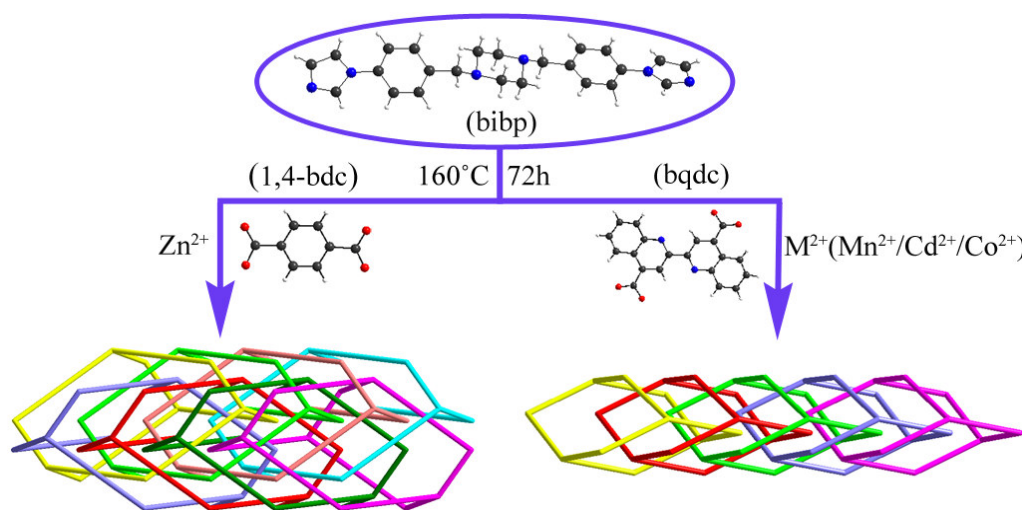
The design and synthesis of entangled metal-organic frameworks (MOFs) have attracted much attention during the past two decades, not only stem from their complicated architectures and various topologies, but also for their intriguing potential applications in many fields as functional materials [1]. As an important subclass of entanglement, interpenetrated frameworks are of great current interest because of their intrinsic aesthetic appeal, and more importantly, due to their potential applications originating from the intertwining nature of the lattices [2]. Diamondoid lattices, which are formed by propagating a tetrahedral nodal point in four directions by coordinating to linear bidentate ligands, are one of the most common types in the interpenetrated coordination networks [3]. So far, a variety of fascinating interpenetrated diamondoid (**dia**) nets with a total degree of interpenetration (hereafter termed Z) from 2 to 12 and 25 have been reported [4].

Nevertheless, the interpenetrated **dia** networks with $Z \geq 5$ are still rare [5]. Moreover, among the currently known examples of interpenetrated **dia** frameworks with $Z \geq 5$ —almost all constructed from single ligands [4a, 4d, 6]—only a few elegant examples with mixed spacer ligands have been reported recently [4b, 4c, 7, 8]. However, close inspection of these structures reveals that the mixed spacer ligands used in building the **dia** frameworks with high degree of interpenetration usually have similar length. To our knowledge, only five 5-fold, two 8-fold and one 9-fold interpenetrating **dia** networks are constructed from mixed spacer ligands with significantly different lengths [8]. This may be attributed, at least in part, to the fact

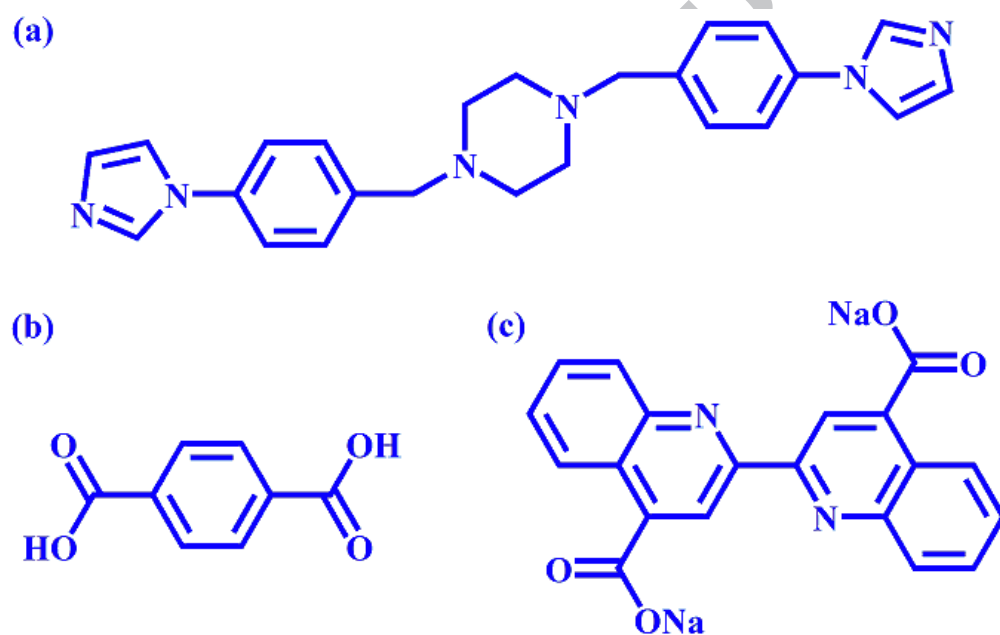
that two linear ligands with significantly different lengths may lead to highly distorted adamantanoid cages containing four cyclohexane-like windows with different sizes. It is known that **dia** net is self-dual, that is to say, **dia** net can interpenetrate in such a way that it is fully catenated. Therefore, when the cyclohexane-like windows of different sizes coexist in the distorted adamantanoid cages, the degree of interpenetration depends on the smallest cyclohexane-like window. The smaller the cyclohexane-like window is in a **dia** net, the lower degree of interpenetration occurs. Consequently, the use of mixed spacer ligands with significantly different lengths to construct interpenetrated **dia** frameworks with $Z \geq 5$ is still a formidable challenge for synthetic chemists, and further research is necessary to enrich and develop this branch.

In order to address this challenge, we purposely focused our attention on a new long linear N-donor ligand 1,4-bis(4-(imidazole-1-yl)benzyl)piperazine (bibp, Scheme 1 and 2a), to produce novel coordination polymers with high degree of **dia** interpenetration in the presence of short ditopic carboxylate linkers, based on the following considerations: (i) Usually, long organic ligands will lead to larger voids which may thus favor the formation of interpenetrated networks [4b]. As evidenced by the report of Champness, Schröder, and co-workers [9], lengthening of linear ligands may increase the fold-interpenetrating number of **dia** networks. The bibp ligand (19.5 Å) is much longer than those N-donor ligands (4,4'-bipyridyl, 7.1 Å; 1,2-trans-(4-pyridyl)ethene, 9.4 Å, etc) used in previously reported interpenetrating **dia** networks [9-10], we thus envision that it should be possible to realize the

relatively high degree of **dia** interpenetration by appropriately combining long bibp ligand and short ditopic carboxylate ligands. (ii) The bibp ligand, a novel long linear semi-flexible ligand with imidazole donors at either end, has never been used to construct coordination compounds; therefore, much work is still necessary to understand the coordination chemistry of bibp. Bearing these considerations in mind, we have performed many experiments, and these efforts have led to the isolation of four new interpenetrated **dia** networks with $Z \geq 5$, namely $[\text{Zn}(\text{1,4-bdc})(\text{bibp})]$ (**1**), $[\text{Mn}(\text{bqdc})(\text{bibp})]$ (**2**), $[\text{Cd}(\text{bqdc})(\text{bibp})]$ (**3**), $[\text{Co}_4(\text{bqdc})_4(\text{bibp})_4]$ (**4**) (1,4-bdc = 1,4-benzenedicarboxylate, bqdc = 2,2'-biquinoline-4,4'-dicarboxylate, Scheme 1 and 2). Compounds **1-4** have several unusual features: (1) The unusual 8-fold (4+4) interpenetrated **dia** net of **1** contains unique quadruple-stranded intertwined homo-axis helices, which can also be considered as an inextricable quadruple-stranded braid. (2) The octuple-stranded braid constructed from two interwoven quadruple-stranded braids in compound **1** is unprecedented. (3) The 5-fold interpenetrating **dia** networks of **2-4** incorporate exceptional quintuple-stranded molecular braid.



Scheme 1. Synthetic conditions for compounds 1-4.



Scheme 2. Schematic drawing of (a) bibp, (b) 1,4-H₂bdc and (c) Na₂bqdc ligands.

Experimental

Materials and general methods

All of the available chemicals and solvents were commercially purchased and used as received without further purification.

Elemental analyses (C, H and N) were performed on a Perkin-Elmer 2400 CHN Elemental Analyzer. Zn, Mn, Cd and Co were determined by a tps-7000 Plasma-Spec(I) inductively coupled plasma-atomic emission spectrometer (ICP-AES). IR spectra were recorded in the range 400-4000 cm^{-1} on a Bio-Rad FTS-185 FT/IR Spectrophotometer using KBr pellets. TG analyses were performed on a NETZSCH STA 449C instrument in flowing N_2 with a heating rate of 10 $^\circ\text{C}\cdot\text{min}^{-1}$. XRPD data were recorded on a XD-3 diffractometer using Cu $\text{K}\alpha$ radiation. Excitation and emission spectra were performed on an F-7000 FL fluorescence spectrophotometer equipped with a 150 W xenon lamp as the excitation source. Variable-temperature magnetic susceptibility data were obtained on a SQUID magnetometer (Quantum Design, MPMS-7) in the temperature range of 2–300 K with an applied field of 1.0 kOe.

Preparation

Synthesis of bibp. A mixture of anhydrous piperazine (0.1 mol, 8.6 g), 1-bromo-4-(bromomethyl)benzene (0.2 mol, 50.0 g), and K_2CO_3 (0.2 mol, 27.6 g) in 1000 mL DMF was refluxed for three days and then poured into 5000 mL H_2O (Scheme S1). The obtained precipitate was crystallized in methanol to give 1,4-bis(4-bromobenzyl)piperazine (79% yield). Elemental analysis (%) calcd for $\text{C}_{18}\text{H}_{20}\text{Br}_2\text{N}_2$: C, 50.97; H, 4.75; N, 6.60 %. Found: C, 50.75; H, 4.58; N, 6.41 %.

A mixture of 1,4-bis(4-bromobenzyl)piperazine (0.1 mol, 42.4 g), imidazole (0.4 mol, 27.2 g), copper(II) sulfate pentahydrate (4 mmol, 1.0 g), and K_2CO_3 (0.2 mol, 27.6 g) in 1000 mL DMF was refluxed for 12 hours and then poured into 2000 mL

H₂O (Scheme S1). The obtained precipitate was crystallized in methanol to give bibp ligand (65% yield). EI-MS: m/z [M-H]⁺, 399.22 (calcd for C₂₄H₂₆N₆, 398.22). Elemental analysis (%) calcd for C₂₄H₂₆N₆: C, 72.33; H, 6.58; N, 21.09 %. Found: 72.08; H, 6.39; N, 20.92 %. FT/IR data (cm⁻¹): 3424(br), 3101(w), 2968(w), 2949(w), 2811(m), 2764(w), 2660(w), 1630(s), 1605(s), 1523(s), 1488(w), 1458(w), 1397(m), 1349(m), 1301(m), 1284(w), 1265(w), 1247(w), 1110(m), 1059(m), 1012(w), 995(w), 857(w), 835(w), 740(m), 665(m), 539(m).

Synthesis of [Zn(1,4-bdc)(bibp)] (1). A mixture of Zn(Ac)₂·2H₂O (0.088 g, 0.4 mmol), 1,4-H₂bdc (0.034 g, 0.2 mmol), bibp (0.080 g, 0.2 mmol), Et₃N (0.25 mL) and distilled water (10 mL) was stirred about 15 min in air, then transferred and sealed in a 17 mL Teflon-lined autoclave, which was heated at 160 °C for 72 h. After slow cooling to room temperature, light yellow block crystals of **1** were filtered off, washed with distilled water, and dried at ambient temperature (yield: 45% based on Zn). Elemental analysis (%) calcd for C₃₂H₃₀ZnN₆O₄: C, 61.21; H, 4.81; N, 13.38; Zn, 10.41 %. Found: C, 61.47; H, 4.62; N, 13.21; Zn, 10.63 %. FT/IR data (cm⁻¹): 3443(br), 3129(w), 3040(w), 2953(w), 2906(m), 2804(m), 2767(m), 2726(m), 2699(m), 1889(w), 1608(s), 1523(s), 1499(m), 1460(m), 1434(m), 1342(s), 1305(s), 1268(m), 1245(m), 1152(m), 1125(s), 1107(m), 1064(s), 1007(m), 964(m), 947(m), 885(w), 849(m), 823(m), 801(m), 764(m), 746(s), 654(m), 621(w), 574(m), 527(m), 500(w), 427(w).

Synthesis of [Mn(bqdc)(bibp)] (2). A mixture of Mn(Ac)₂·4H₂O (0.049 g, 0.2 mmol), Na₂bqdc (0.039 g, 0.1 mmol), bibp (0.040 g, 0.1 mmol), Et₃N (0.20 mL) and distilled

water (10 mL) was stirred about 15 min in air, then transferred and sealed in a 17 mL Teflon-lined autoclave, which was heated at 160 °C for 72 h. After slow cooling to room temperature, light yellow block crystals of **2** were filtered off, washed with distilled water, and dried at ambient temperature (yield: 46% based on Mn). Elemental analysis (%) calcd for $C_{44}H_{36}MnN_8O_4$: C, 66.41; H, 4.56; N, 14.08; Mn, 6.90 %. Found: C, 66.18; H, 4.39; N, 14.33; Mn, 7.11 %. FT/IR data (cm^{-1}): 3411(br), 3159(m), 3139(m), 3120(s), 2940(w), 2816(m), 2800(m), 2769(w), 2690(w), 1599(w), 1556(s), 1536(s), 1517(s), 1500(m), 1456(m), 1418(s), 1372(s), 1307(s), 1288(m), 1258(w), 1153(m), 1129(m), 1116(s), 1066(s), 1013(w), 965(w), 933(m), 834(m), 815(m), 787(s), 762(m), 667(w), 635(s), 621(w), 597(w), 540(m), 525(m), 487(w), 453(w), 415(w).

Synthesis of [Cd(bqdc)(bibp)] (3). The preparation of **3** was similar to that of **2** except that $Cd(Ac)_2 \cdot 2H_2O$ (0.054 g, 0.2 mmol) was used instead of $Mn(Ac)_2 \cdot 4H_2O$. Colorless block crystals of **3** were collected (yield: 41% based on Cd). Elemental analysis (%) calcd for $C_{44}H_{36}CdN_8O_4$: C, 61.94; H, 4.25; N, 13.13; Cd, 13.17 %. Found: C, 62.19; H, 4.11; N, 12.94; Cd, 13.35 %. FT/IR data (cm^{-1}): 3439(br), 3117(w), 3044(w), 2910(m), 2800(m), 2771(m), 1598(m), 1557(s), 1537(s), 1519(s), 1456(m), 1416(m), 1367(s), 1307(s), 1288(m), 1238(m), 1200(m), 1153(m), 1119(s), 1012(m), 964(m), 932(m), 886(w), 836(m), 814(m), 787(s), 763(m), 666(m), 539(w), 525(w), 487(w), 416(w).

Synthesis of [Co₄(bqdc)₄(bibp)₄] (4). A mixture of $Co(Ac)_2 \cdot 4H_2O$ (0.100 g, 0.4 mmol), Na_2bqdc (0.078 g, 0.2 mmol), bibp (0.080 g, 0.2 mmol), Et_3N (0.25 mL) and

distilled water (10 mL) was stirred about 15 min in air, then transferred and sealed in a 17 mL Teflon-lined autoclave, which was heated at 160 °C for 72 h. After slow cooling to room temperature, dark purple block crystals of **4** were filtered off, washed with distilled water, and dried at ambient temperature (yield: 43% based on Co). Elemental analysis (%) calcd for C₁₇₆H₁₄₄Co₄N₃₂O₁₆: C, 66.08; H, 4.51; N, 14.02; Co, 7.38 %. Found: C, 66.32; H, 4.33; N, 13.83; Co, 7.54 %. FT/IR data (cm⁻¹): 3402(br), 3121(m), 2944(w), 2805(m), 2373(w), 1603(m), 1562(s), 1521(s), 1419(s), 1367(s), 1306(s), 1237(m), 1200(m), 1154(m), 1119(s), 1062(s), 1009(m), 965(w), 933(m), 885(w), 844(m), 814(s), 785(s), 761(m), 736(w), 666(m), 653(m), 601(w), 526(m), 486(w), 425(w).

X-Ray crystallography

Suitable single crystals of **1-4** were selected for single-crystal X-ray diffraction analysis (diffractometer device type: SuperNova, Dual, Cu at zero, EosS2). Compounds **1-4** were collected with Cu K α radiation ($\lambda = 1.54184 \text{ \AA}$) at 289 K, 284.5 K, 284.5 K and 290 K, respectively. Using Olex2 [11], the structures of **1** and **3** were solved with the ShelXS [12] structure solution program using Direct Methods, while the structures of **2** and **4** were solved with the Superflip [13] structure solution program using Charge Flipping. Moreover, the structures of **1-4** were refined with the ShelXL [12] refinement package using Least Square minimization. All non-hydrogen atoms were refined anisotropically. The organic hydrogen atoms were generated geometrically. The disordered C atoms (C20, C21) of bibp ligand in compound **1** were refined using C atoms split over two sites, with a total occupancy of 1. The crystal

data and structure refinement of compounds **1-4** are summarized in Table 1. Selected bond lengths for **1-4** are listed in Table S1. The topological analyses were done with the TOPOS program [14].

Table 1 Crystal data and structure refinements for compounds **1-4**.

Compound	1	2	3	4
Empirical formula	C ₃₂ H ₃₀ N ₆ O ₄ Zn	C ₄₄ H ₃₆ MnN ₈ O ₄	C ₄₄ H ₃₆ CdN ₈ O ₄	C ₁₇₆ H ₁₄₄ Co ₄ N ₃₂ O ₁₆
<i>M_r</i> (g mol ⁻¹)	627.99	795.75	853.21	3198.94
Crystal system	Orthorhombic	Monoclinic	Monoclinic	Triclinic
Space group	<i>Pna</i> 2 ₁	<i>P</i> 2 ₁ / <i>n</i>	<i>P</i> 2 ₁ / <i>n</i>	<i>P</i> $\bar{1}$
<i>a</i> (Å)	15.8128(2)	13.7817(2)	13.805(4)	16.1255(8)
<i>b</i> (Å)	12.2565(1)	17.4459(2)	17.346(3)	22.960(2)
<i>c</i> (Å)	15.4615(2)	17.0228(3)	17.465(4)	23.044(2)
α (°)	90	90	90	107.831(9)
β (°)	90	109.507(2)	110.57(3)	100.641(6)
γ (°)	90	90	90	100.815(6)
<i>V</i> (Å ³)	2996.61(5)	3857.95(10)	3915.8(18)	7705.7(12)
<i>Z</i>	4	4	4	2
ρ_{calcd} (g·cm ⁻³)	1.392	1.370	1.447	1.377
μ (mm ⁻¹)	1.527	3.233	4.911	3.943
<i>F</i> (000)	1304.0	1652.0	1744.0	3310.0
2 θ range/°	9.128-143.066	8.794-143.284	8.72-144.862	7.956-134.158
Reflections collected	41888	27458	21366	69362
Unique data (<i>R</i> _{int})	5815 (0.0385)	7336 (0.0420)	7115 (0.0327)	27111 (0.0392)
GOF on <i>F</i> ²	1.044	1.015	1.073	1.101
<i>R</i> ₁ ^a / <i>wR</i> ₂ ^b [<i>I</i> > 2 σ (<i>I</i>)]	0.0311/0.0873	0.0492/0.1188	0.0355/0.0799	0.1306/0.3165
<i>R</i> ₁ ^a / <i>wR</i> ₂ ^b (all data)	0.0315/0.0879	0.0637/0.1275	0.0476/0.0841	0.1467/0.3251

$$^a R_1 = \sum \|F_o\| - |F_c| / \sum \|F_o\|; ^b wR_2 = \sum [w(F_o^2 - F_c^2)^2] / \sum [w(F_o^2)^2]^{1/2}$$

Results and discussion

Crystal structure of **1**

Single crystal X-ray diffraction analysis reveals that **1** crystallizes in the polar space group *Pna*2₁ and exhibits an 8-fold [4+4] interpenetrating **dia** network containing the exceptional quadruple-stranded homo-axis helices. The asymmetric unit of **1** consists of one Zn(II) ion, one 1,4-bdc ligand and one bibp ligand. As shown in Fig. 1, the

coordination environment around Zn1 can be described as a distorted tetrahedral geometry, being coordinated by two carboxylate oxygen atoms (Zn-O 1.946(2) and 1.972(3) Å) from two different 1,4-bdc ligands and two nitrogen atoms (Zn-N 2.029(3) and 2.009(2) Å) from two different bibp ligands. In addition, each long ligand, bibp acts as a linear bridging ligand connecting two Zn atoms, so does each 1,4-bdc ligand (Scheme S2). Based on these connection modes, each Zn center acts as a tetrahedral node and is linked to four equivalent neighbors through four linear ligands into a 3D **dia** network (Fig. 2b). Due to the different lengths of the mixed spacer ligands, a single **dia** network contains highly distorted adamantane-like cages, in which the distances between two Zn atoms connected by 1,4-bdc ligand and bibp are 10.907 Å and 22.854 Å, respectively. This results in a single adamantanoid cage delineated by two types of cyclohexane-like windows with different sizes (two big windows 43.84 Å × 38.71 Å, two small windows 33.52 Å × 28.58 Å, Fig. 2a). The dimension of the adamantanoid cages is 49.03 Å × 39.46 Å × 31.63 Å (corresponding to the longest intracage Zn...Zn distances). Although the fold-interpenetrating number of **dia** networks rests with the small cyclohexane-like window of adamantanoid cage, the large size of the small cyclohexane-like window still makes the interpenetration of eight identical **dia** networks possible to give an intricate 8-fold interpenetrating **dia** array (Fig. 2c). So far, the interpenetrated **dia** networks constructed from mixed spacer ligands with $Z \geq 8$ are still quite uncommon, and only six 8-fold, one 9-fold and two 10-fold interpenetrating **dia** nets formed from mixed spacer ligands have been reported [4c, 7a, 7c-7e, 8f, 8g]. However, among them, only two 8-fold and one 9-fold

networks constructed from mixed spacer ligands with significantly different lengths [8f, 8g]. Undoubtedly, the successful isolation of compound **1** adds a new member to the family of highly interpenetrated **dia** nets constructed from mixed spacer ligands with significantly different lengths. More intriguingly, an analysis of the interpenetration topology with the TOPOS program reveals that **1** belongs to rare class IIIa (the whole interpenetrated array is generated both by translations and by non-translating interpenetration symmetry elements (NISE)) with $Z_t = 4$ and $Z_n = 2$. In detail, four **dia** nets are generated by application of one translational operation and the translating interpenetration vector (TIV) is $[0,1,0]$ (12.25 Å, Fig. S1). The presence of a NISE as the 2_1 screw axis along the c axis generates a second set of four **dia** nets for a total degree of interpenetration of class IIIa of $8 = [4 \times 2]$ (Fig. S2). There are twelve examples containing [4+4] interpenetrating **dia** nets to date [6c, 6e, 6f, 6i-k, 7d, 8f], but only three structures belong to class IIIa (CSD refcode: FISPIH, OTUXIL, ZOZSEO, Table S2). The non-translational symmetry elements (inversion center) in aforementioned three **dia** nets obviously differ from that in **1**. Thus compound **1** shows an unprecedented interpenetration mode among [4+4] interpenetrating **dia** nets. In addition, a small window is threaded by two neighboring small windows belonging to two other nets (Fig. S3). To the best of our knowledge, this phenomenon is really scarce in interpenetrated **dia** networks.

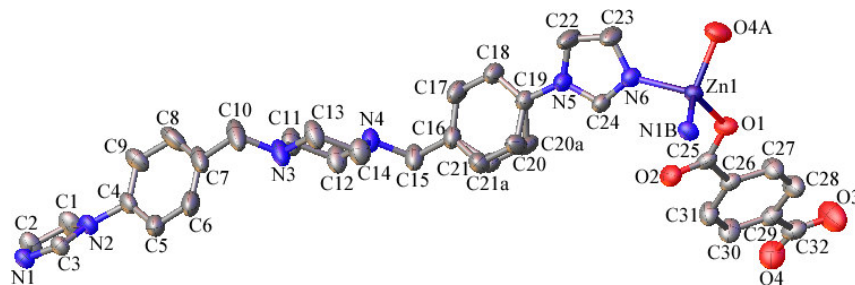


Fig. 1. ORTEP diagram showing the coordination environment for Zn atoms in **1** (all hydrogen atoms are omitted for clarity).

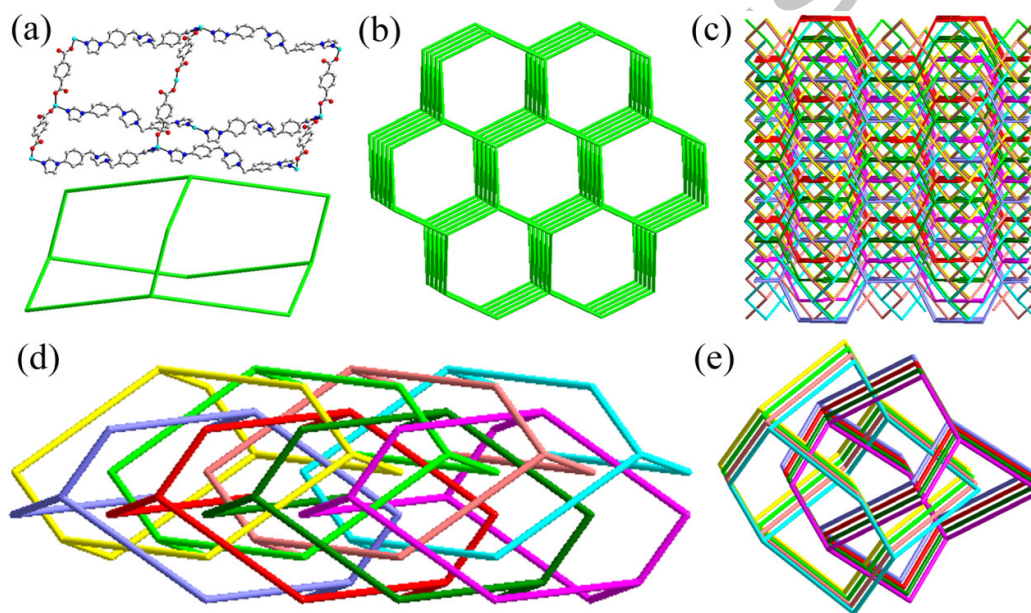


Fig. 2. For compound **1**: (a) Perspective (upper) and simplified (down) views of a single adamantanoid cage. (b) A single 3D-diamondoid network showing large voids. (c) View of the 8-fold interpenetrated 3D framework and individual networks are displayed in different colors. (d) Topological representation of the 8-fold interpenetrated nets. (e) The schematic representation of [4+4] mode of diamondoid interpenetration.

The most striking structural feature of **1** is the existence of the unique quadruple-stranded intertwined homo-axis helices, which can also be considered as an uncommon quadruple-stranded braid. As depicted in Fig. S4, the Zn atoms are bridged by 1,4-bdc and bibp ligands to form the left- and right-handed helical chains running along a crystallographic 2_1 axis in the a direction with a pitch of 31.661 Å. Unexpectedly, four such helical chains, which possess the same helix axis and have the reverse helical orientation, interweave each other to produce a fascinating quadruple-stranded homo-axis helices without sharing the atoms, in contrast to the previous homo-axis helices those have interweaving of different kinds (or same kind) of helices sharing the atoms [15]. To our knowledge, the quadruple-stranded homo-axis helices represent the highest-stranded homo-axis helices involving left-handed and right-handed helices without sharing the atoms. Moreover, careful inspection of the quadruple-stranded homo-axis helices reveals that these helices can be further classified into left-handed (yellow and pink helices, Figs. 3c and 3d) and right-handed double helices (red and purple helices, Figs. 3c and 3d) according to the helical orientation. Interestingly, the left-handed double helices are further intertwined with the right-handed double helices in such a way that two helices of one double helical strand pass through the openings generated by the other double helices, in a mutual relationship (Figs. S5a and S5b). Thus, the quadruple-stranded homo-axis helices could equally well be considered as a quadruple-stranded braid. To the best of our knowledge, only one example containing peculiar quadruple-stranded braid motif has been reported by Wang and coworkers [16]. However, in contrast to the

quadruple-stranded braid motif reported in ref. 16, where two helices of a side-by-side double helix are separated from each other, arbitrary two helices of the quadruple-stranded braid motif in **1** interweave each other (Fig. S6). Furthermore, we have carefully studied all 8-fold [4+4] interpenetrated **dia** coordination networks, and none of them contains the quadruple-stranded braid involving left-handed and right-handed double helices without sharing the atoms indeed. Another noteworthy aspect of the quadruple-stranded braid motif in **1** is the fact that the left-handed helix is intertwined with right-handed helix without sharing the atoms to generate an exceptional double helix (Fig. S7), which is a new structural motif that has never been observed prior to this work. Therefore, this more inextricable quadruple-stranded braid motif represents a new type of entanglement of the one-dimensional (1D) chains. Most exciting is the fact that two adjacent quadruple-stranded braids further intertwine with each other to generate other openings which are penetrated by two helical chains (Figs. S5c and S5d). This results in a more complicated 8-stranded interwoven braid derived from eight individual **dia** networks (Figs. 3a and 3b). According to our careful check, so far such an 8-stranded interwoven braid has never been observed in any 8-fold interpenetrated **dia** network. It is believed that such an exceptional 8-stranded interwoven braid is derived from the unprecedented interpenetration mode in compound **1**.

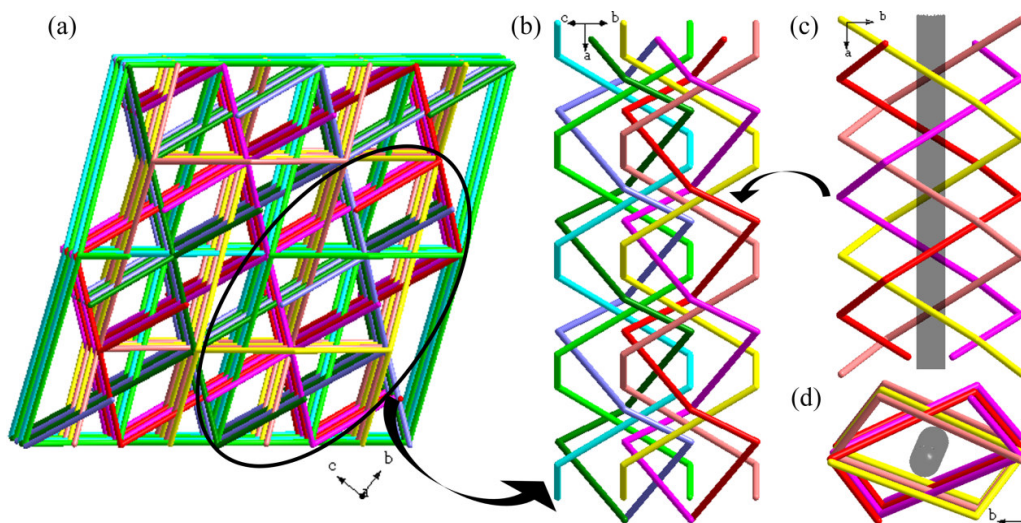


Fig. 3. For compound **1**: (a) View of the 8-fold interpenetrated 3D framework along a axis. (b) Schematic view of the 8-stranded interwoven braid. (c) Schematic view of the quadruple-stranded intertwined homo-axis helices along c axis. (d) Side view of the quadruple-stranded intertwined homo-axis helices along a axis.

Crystal structures of 2-4

When 1,4-bdc was replaced by bqdc, three 5-fold interpenetrating **dia** networks were obtained. Compounds **2** and **3** are isostructural, while compound **4** is isorecticular to them owing to the same network topology [17], so only the structure of **2** will be discussed in detail. There is one crystallographically independent Mn atom in the asymmetric unit of **2** (Fig. 4). Each Mn atom is coordinated by four oxygen atoms (Mn-O 2.1813(17)-2.3374(19) Å) from two chelating carboxylate group of different bqdc ligands and two nitrogen atoms (Mn-N 2.197(2) and 2.213(2) Å) from two bibp ligands, showing a distorted octahedral geometry. Moreover, the bibp acts as a linear bidentate ligand linking the adjacent two Mn(II) atoms, while the bqdc ligand adopts a

bis(bidentate) coordination mode to bridge two Mn(II) atoms (Scheme S2). On the basis of these connection modes, each Mn(II) atom, which corresponds to a tetrahedral node, is connected to four others through two bibp and two bqdc ligands to generate a 3D **dia** network (Fig. S9). Owing to the significantly different lengths of the two types of ligands, the distorted adamantanoid cage in a single **dia** network contains two types of cyclohexane-like windows with different sizes (two big windows $46.63 \text{ \AA} \times 45.14 \text{ \AA}$, two small windows $34.87 \text{ \AA} \times 31.21 \text{ \AA}$, Fig. S9a), and exhibits maximum dimensions of $51.981 \text{ \AA} \times 49.271 \text{ \AA} \times 17.446 \text{ \AA}$ (corresponding to the longest intracage Mn...Mn distances). Although the small cyclohexane-like window may determine the degree of interpenetration for **dia** networks, the large size of the small cyclohexane-like window still allows a relatively high degree of interpenetration to occur. As illustrated in Fig. 5, a single **dia** network is interpenetrated by four other identical **dia** networks in a normal mode to give a 5-fold interpenetrating **dia** networks [1a, 6i]. Compared to **1**, the relatively low degree of interpenetration in **2** is related to the fact that the steric hindrance of bqdc ligand is larger than that of 1,4-bdc ligand. An analysis of the interpenetration topology with the TOPOS program reveals that it belongs to class Ia, that is, the five identical interpenetrated nets are generated only by translation and the translating vector is $[1,0,0]$ (13.78 \AA).

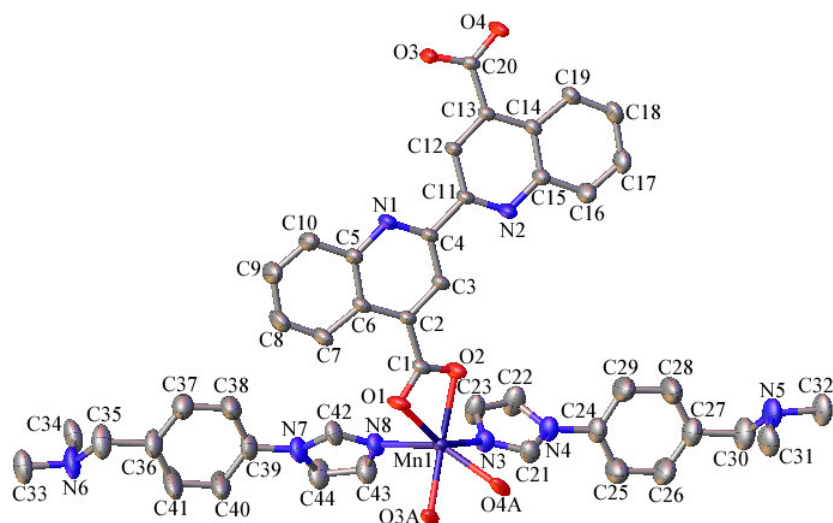


Fig. 4. ORTEP diagram showing the coordination environment for Mn atoms in **2** (all hydrogen atoms are omitted for clarity).

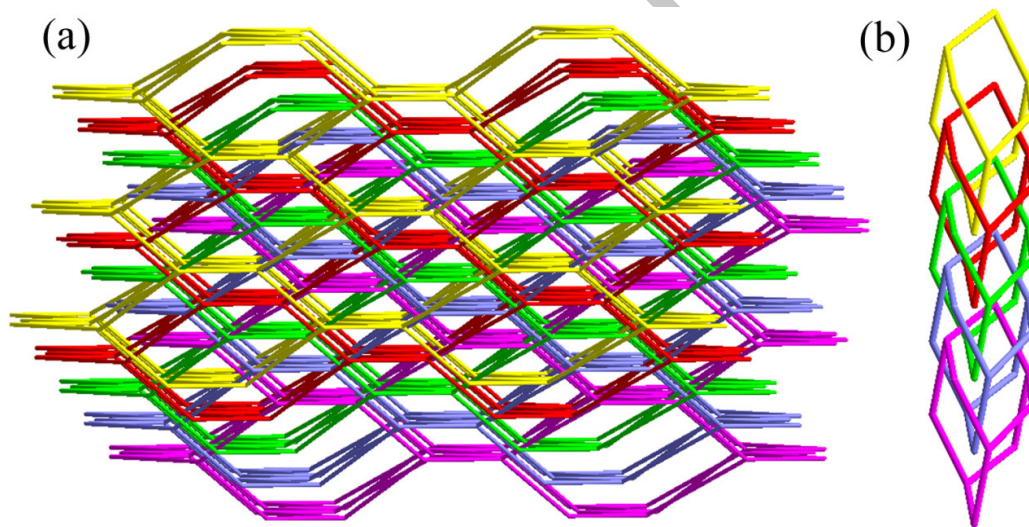


Fig. 5. For compound **2**: (a) View of the 5-fold interpenetrated 3D framework and individual networks are displayed in different colors. (b) Topological representation of the 5-fold interpenetrated networks.

The most fascinating structural feature of **2** is that an exceptional quintuple-stranded molecular braid (also called a quintuple-stranded meso-helix [18])

originating from five individual **dia** nets exists in the 5-fold interpenetrated nets of **2**. As shown in Fig. 6, the quintuple-stranded molecular braid is formed by bibp and bqdc ligands bridging the Mn(II) atoms, which is extended along the crystallographic *a* axis with a pitch of 68.909 Å. Up to now, the occurrence of molecular braids is strikingly rare, and only a handful of molecular braids have been reported [19]. To the best of our knowledge, compound **2** represents the second quintuple-stranded molecular braid in the field of coordination polymers, and it also represents the highest-stranded molecular braid without sharing the metal atoms [18, 20].

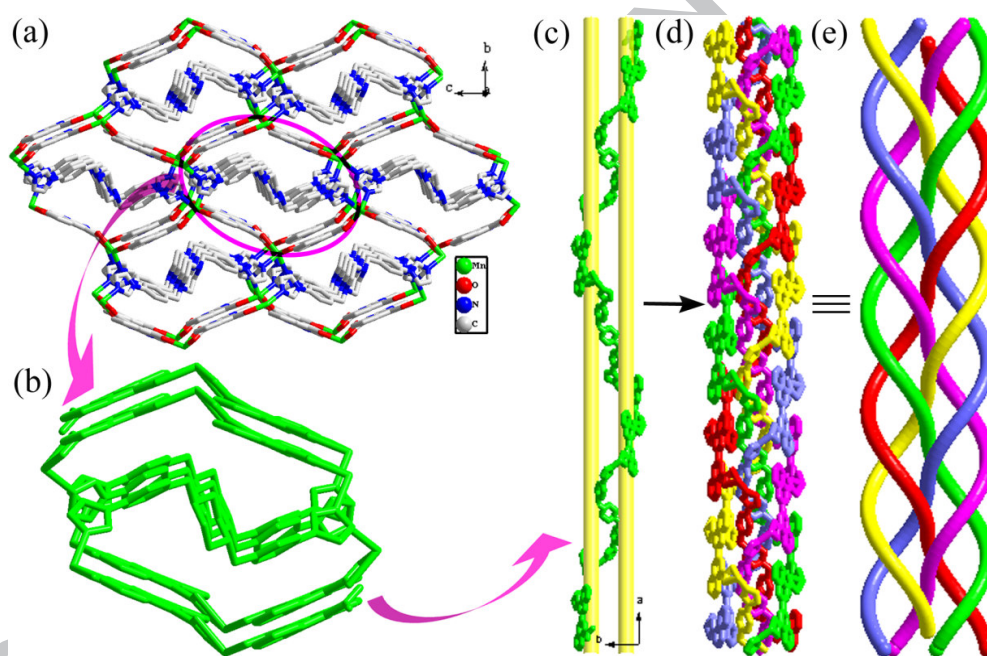


Fig. 6. For compound **2**: (a) Perspective view of a single 3D net. (b) Side view of the single-stranded *meso*-helix. (c) Perspective view of the *meso*-helix. (d) Perspective view of the quintuple-stranded molecular braid. (e) Schematic view of the quintuple-stranded molecular braid.

Comparison of compounds 1–4 the factors influencing interpenetration

As shown above, the simultaneous use of long bibp ligand and short ditopic carboxylate ligands affords four new interpenetrated **dia** networks with $Z \geq 5$. Although it is difficult to predict and explain the degree of interpenetration with our present state of knowledge, some of the influence factors observed are discussed below.

As described above, because **dia** net is self-dual, the degree of interpenetration for **dia** nets rests with the smallest cyclohexane-like window of adamantanoid cage, which is evidenced by the analysis of the structures of **1-4**. Furthermore, the comparison of compound **1** with **2-4** also shows that the bulkiness of the ligands is another factor that can affect the fold-interpenetrating number of **dia** networks. Because bqdc ligand is larger than 1,4-bdc ligand, the free aperture of smallest cyclohexane-like windows in **2** (dimensions: 22.54 Å × 11.25 Å, considering van der Waals radii; Fig. S12a) is smaller than that in **1** (dimensions: 22.86 Å × 17.00 Å, Fig. S12b). This leads to the lower degree of interpenetration in compound **2**. By careful inspection of the structures of **1-4**, we can see the trend that the decrease in the free aperture of smallest cyclohexane-like window induces the progressive decrease in the fold-interpenetrating number of **dia** networks. Similar trend has also been observed in a series of interpenetrated **dia** networks [Ag(ddn)₂]X (ddn = 1,12-dodecanedinitrile; X = NO₃⁻, PF₆⁻, AsF₆⁻, ClO₄⁻) (Fig. S13) [6i]. Looking at the entire study, we can sense that the length ratio of mixed spacer ligands and the ratio of length to bulkiness of the ligand, which can modulate the free aperture of smallest cyclohexane-like window,

play important roles in tuning the degree of **dia** interpenetration.

X-Ray powder diffractions and thermal properties

In order to check the phase purity of compounds **1-4**, the X-ray powder diffraction (XRPD) patterns were recorded at room temperature. As shown in Figs. S14-S17, the peak positions of simulated and experimental patterns are in good agreement with each other, demonstrating the phase purity of the products. The differences in intensity may be due to the preferred orientation of the crystalline powder samples.

Thermal gravimetric analyses (TG) were performed on compounds **1-4** to investigate their thermal stabilities. The TG curves of **1-4** are highly similar (Figs. S18-S21). The release of organic components occurs from 390 °C for **1**, 400 °C for **2**, 390 °C for **3**, and 370 °C for **4**. For compounds **1-4**, the total weight losses of 76.39%, 72.64%, 79.46%, 74.28% are much less than the calculated value of 87.04%, 91.09%, 84.95%, 90.62% if the final products are assumed to be ZnO, MnO, CdO, CoO, respectively, which indicates that the decomposing processes are not complete due to the use of nitrogen protection. In their DSC curves (Figs. S18-S21), the endothermic peak at 431 °C and the exothermic peaks at 543 °C, 641 °C for **1**, the endothermic peak at 420 °C and the exothermic peak at 669 °C for **2**, the endothermic peak at 429 °C and the exothermic peak at 632 °C for **3**, the endothermic peak at 399 °C and the exothermic peak at 530 °C for **4**, are all related to the decomposition of the organic ligands.

Photoluminescence properties

Taking into account the excellent luminescent properties of d^{10} metal complexes,

the solid-state luminescence of **1**, **3** and organic ligands were investigated (Figs. 7a and 7b). The 1,4-H₂bdc, Na₂bqdc and bibp ligands exhibit the fluorescent emission bands at 383 nm ($\lambda_{\text{ex}} = 282$ nm), 431 nm ($\lambda_{\text{ex}} = 284$ nm) and 378 nm ($\lambda_{\text{ex}} = 315$ nm) respectively, which are probably caused by the $\pi^* \rightarrow n$ or $\pi^* \rightarrow \pi$ transition [21]. Compound **1** exhibits an intense emission at 444 nm in the blue region upon excitation at 372 nm. Compared with the 1,4-H₂bdc ligand and the bibp ligand, it can be seen that the maximum emission peak of **1** has a remarkable bathochromic shift. Therefore, the emission of **1** may not be related to the $\pi^* \rightarrow n$ or $\pi^* \rightarrow \pi$ transition of the ligand. According to the previous literature, this emission could be assigned to ligand-to-metal charge transfer (LMCT) [21d, 22]. Compound **3** emits intense blue fluorescent emission at 427 nm with an excitation at 201 nm. Compared with the Na₂bqdc ligand and the bibp ligand, the emission spectrum of **3** is similar to that of Na₂bqdc. Thus, the emission of compound **3** may be attributed to the intraligand fluorescent emission.

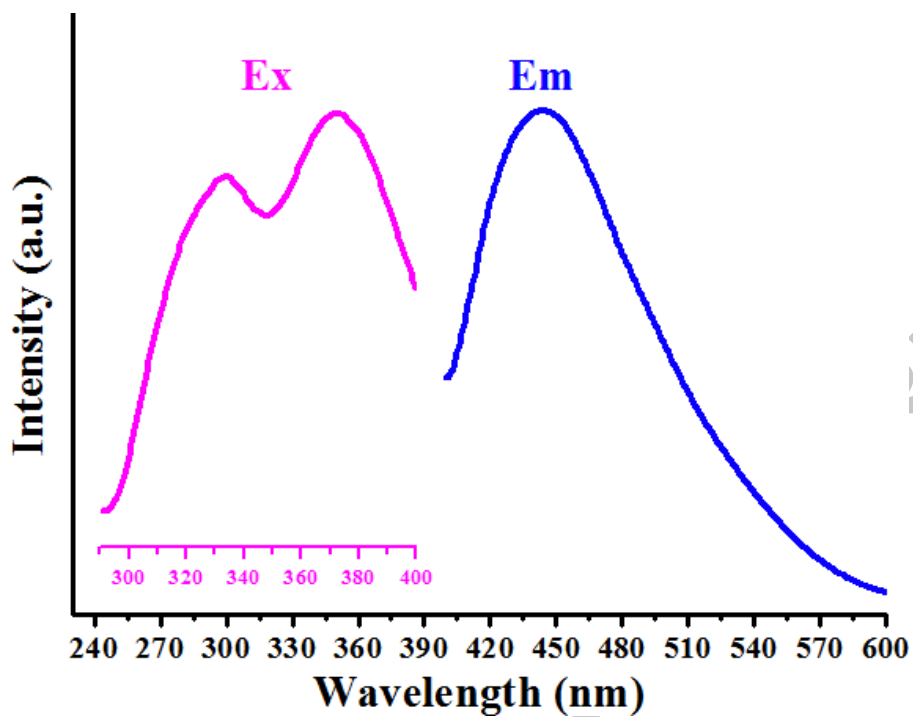


Fig. 7a

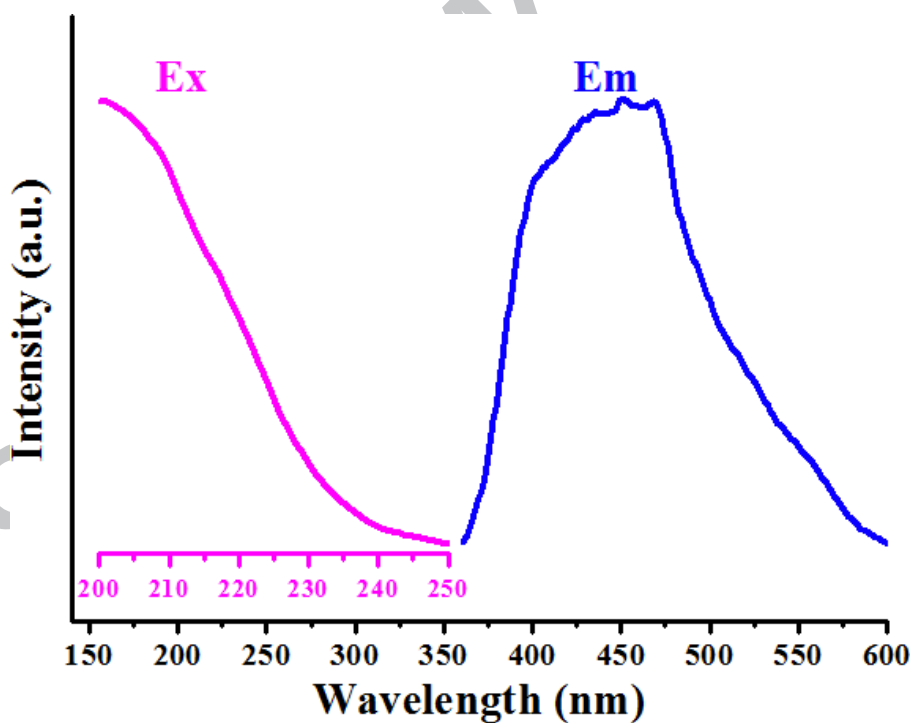


Fig. 7b

Fig. 7. Photoluminescent spectra of **1** (a) and **3** (b) in solid state at room temperature.

Magnetic properties

The temperature dependence of the magnetic susceptibility of **4** was studied in the temperature range of 2-300 K at a direct current field of 1.0 kOe. As shown in Fig. 8, the $\chi_M T$ value of $11.714 \text{ cm}^3 \text{ K mol}^{-1}$ at 300 K ($9.680 \mu_B$) is much higher than the expected value of $7.5 \text{ cm}^3 \text{ K mol}^{-1}$ ($7.746 \mu_B$) for four isolated spin-only Co(II) ions ($S = 3/2$, $g = 2.0$), which can be ascribed to the strong orbital contribution to the magnetic moment of Co(II) centers [23]. With decreasing temperature, the $\chi_M T$ product decreases continuously to a value of $6.673 \text{ cm}^3 \text{ K mol}^{-1}$ at 2 K, which is attributed to weak antiferromagnetic interaction between the Co^{II} ions and/or ZFS of Co^{II}. The $1/\chi_M$ versus T plot of **4** follows the Curie-Weiss law in the range of 2-300 K with $C = 10.830 \text{ cm}^3 \text{ K mol}^{-1}$ and $\theta = -3.470 \text{ K}$.

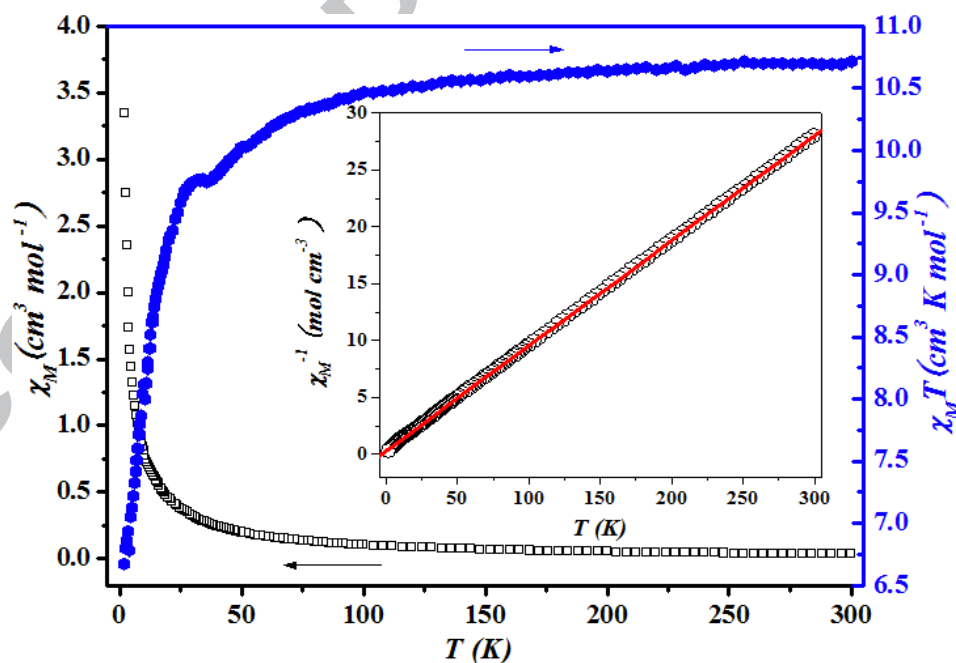


Fig. 8. Temperature dependence of the $\chi_M T$ product for compound **4**. Inset: Plot of thermal variation of χ_M^{-1} for the respective compound.

Conclusions

In summary, we have successfully synthesized and characterized four novel interpenetrated **dia** networks with $Z \geq 5$ by appropriately combining long bibp ligand and short ditopic carboxylate ligands. Compound **1** is an 8-fold [4+4] interpenetrated **dia** network containing uncommon quadruple-stranded homo-axis helices and octuple-stranded braid, which fill the lacunas in the realm of entanglement. Compounds **2-4** display 5-fold interpenetrating **dia** networks comprising an exceptional quintuple-stranded molecular braid. By inspection of the structures of **1-4**, it is believed that tuning of the free aperture of smallest cyclohexane-like window by modulating the length ratio of mixed spacer ligands and the ratio of length to bulkiness of the ligand can adjust the fold-interpenetrating number of **dia** networks. Therefore, the successful isolation of these solid materials provides not only innovative examples of interpenetrated **dia** networks, but also some guidance in controlling and tuning the degree of **dia** interpenetration.

Acknowledgments

This work was financially supported by the NSFC (21571149), the Program for Chongqing Excellent Talents in University, the Fundamental Research Funds for the Central Universities (XDJK2013A027, XDJK2016C101), the Open Fund of Key Laboratory of Synthetic and Natural Functional Molecule Chemistry of the Ministry of Education (338080045).

Appendix A. Supplementary materials

CCDC 1041635 (1), 1054320 (2), 1054328 (3) and 1054331 (4) contain the supplementary crystallographic data for this paper. These data can be obtained free of charge from The Cambridge Crystallographic Data Centre via www.ccdc.cam.ac.uk/data_request/cif. Some additional structural figures and tables, XRPD patterns, TG-DSC curves, IR spectrum, and additional details for single-crystal structural refinements can be found in the supporting file.

Notes and references

- (1) (a) S. R. Batten, *CrystEngComm* 3 (2001) 67; (b) O. M. Yaghi, M. O'Keeffe, N. W. Ockwig, H. K. Chae, M. Eddaoudi, J. Kim, *Nature* 423 (2003) 705; (c) R. Kitaura, K. Seki, G. Akiyama, S. Kitagawa, *Angew. Chem. Int. Ed.* 42 (2003) 428; (d) E. R. Parnham, R. E. Morris, *Acc. Chem. Res.* 40 (2007) 1005; (e) D. R. Xiao, H. Y. Chen, D. Z. Sun, J. H. He, S. W. Yan, J. Yang, X. Wang, R. Yuan, E. B. Wang, *Inorg. Chim. Acta* 14 (2012) 2849; (f) L. Wen, W. Shi, X. T. Chen, H. H. Li, P. Cheng, *Eur. J. Inorg. Chem.* (2012) 3562.
- (2) (a) V. A. Blatov, L. Carlucci, G. Ciani, D. M. Proserpio, *CrystEngComm* 6 (2004) 377; (b) D. R. Xiao, D. Z. Sun, J. L. Liu, G. J. Zhang, H. Y. Chen, J. H. He, S. W. Yan, R. Yuan, E. B. Wang, *Eur. J. Inorg. Chem.* (2011) 3656.
- (3) Y. F. Hsu, C. H. Lin, J. D. Chen, J. C. Wang, *Cryst. Growth Des.* 8 (2008) 1094.
- (4) (a) J. Xu, Z. S. Bai, M. S. Chen, Z. Su, S. S. Chen, W. Y. Sun, *CrystEngComm* 11 (2009) 2728; (b) C. M. Nagaraja, B. Ugale, A. Chanthapally, *CrystEngComm*

- 16 (2014) 4805; (c) M. Ahmad, R. Katoch, A. Garg, P. K. Bharadwaj, CrystEngComm 16 (2014) 4766; (d) Y. P. He, Y. X. Tan, J. Zhang, CrystEngComm 14 (2012) 6359.
- (5) E. V. Alexandrov, V. A. Blatov, A. V. Kochetkov, D. M. Proserpio, CrystEngComm 13 (2011) 3947.
- (6) (a) D. K. Kumar, D. A. Jose, A. Das, P. Dastidar, Inorg. Chem. 44 (2005) 6933; (b) G. B. Li, J. R. He, M. Pan, H. Y. Deng, J. M. Liu, C. Y. Su, Dalton Trans. 41 (2012) 4626; (c) Y. L. Liu, Y. P. Wu, D. S. Li, W. W. Dong, C. S. Zhou, J. Solid State Chem. 223 (2015) 38; (d) T. W. Tseng, T. T. Luo, C. C. Tsai, K. L. Lu, CrystEngComm 17 (2015) 2935; (e) Y. P. He, Y. X. Tan, J. Zhang, Inorg. Chem. 52 (2013) 12758; (f) L. J. Li, G. Yuan, L. Chen, D. Y. Du, X. L. Wang, G. J. Xu, H. N. Wang, K. Z. Shao, Z. M. Su, J. Coord. Chem. 64 (2011) 1578; (g) Z. Z. Lu, R. Zhang, Y. Z. Li, Z. J. Guo, H. G. Zheng, Chem. Commun. 47 (2011) 2919; (h) X. S. Wang, H. Zhao, Z. R. Qu, Q. Ye, J. Zhang, R. G. Xiong, X. Z. You, H. K. Fun, Inorg. Chem. 42 (2003) 5786; (i) L. Carlucci, G. Ciani, D. M. Proserpio, S. Rizzato, Chem.-Eur. J. 8 (2002) 1520; (j) R. G. Xiong, J. L. Zuo, X. Z. You, Z. P. Bai, B. F. Abrahams, C. M. Che, H. K. Fun, Chem. Commun. (2000) 2061; (k) K. A. Hirsch, S. R. Wilson, J. S. Moore, Inorg. Chem. 36 (1997) 2960; (l) Y. J. Hao, B. Wu, S. G. Li, C. D. Jia, X. J. Huang, X. J. Yang, CrystEngComm 13 (2011) 215.
- (7) (a) R. Singh, P. K. Bharadwaj, Cryst. Growth Des. 13 (2013) 3722; (b) H. J. Hao, D. Sun, F. J. Liu, R. B. Huang, L. S. Zheng, Cryst. Growth Des. 11 (2011) 5475;

- (c) Y. F. Hou, N. Yan, K. F. Yue, J. T. Shi, T. He, X. Y. Li, *Inorg. Chem. Commun.* 48 (2014) 44; (d) H. Kim, M. P. Suh, *Inorg. Chem.* 44 (2005) 810; (e) L. L. Dang, J. Q. Li, S. J. Liu, M. B. Luo, F. Luo, *Inorg. Chem. Commun.* 45 (2014) 30; (f) J. Yang, J. F. Ma, Y. Y. Liu, S. R. Batten, *CrystEngComm* 11 (2009) 151; (g) Y. Qi, Y. X. Che, J. M. Zheng, *Cryst. Growth Des.* 8 (2008) 3602.
- (8) **5-fold:** (a) D. P. Martin, M. A. Braverman, R. L. LaDuca, *Cryst. Growth Des.* 7 (2007) 2609; (b) D. K. Maity, B. Bhattacharya, R. Mondal, D. Ghoshal, *CrystEngComm* 16 (2014) 8896; (c) D. Liu, Y. J. Chang, J. P. Lang, *CrystEngComm* 13 (2011) 1851; (d) Y. Yang, P. Du, Y. Y. Liu, J. F. Ma, *Cryst. Growth Des.* 13 (2013) 4781; (e) L. L. Wen, L. Zhou, B. G. Zhang, X. G. Meng, H. Qu, D. F. Li, *J. Mater. Chem.* 22 (2012) 22603; **8/9-fold:** (f) Y. Gong, J. Li, J. Qin, T. Wu, R. Cao, J. Li, *Cryst. Growth Des.* 11 (2011) 1662; (g) J. J. Cheng, Y. T. Chang, C. J. Wu, Y. F. Hsu, C. H. Lin, D. M. Proserpio, J. D. Chen, *CrystEngComm* 14 (2012) 537.
- (9) A. J. Blake, N. R. Champness, S. S. M. Chung, W. S. Li, M. Schroder, *Chem. Commun.* (1997) 1005.
- (10) L. F. Ma, X. Q. Li, Q. L. Meng, L. Y. Wang, M. Du, H. W. Hou, *Cryst. Growth Des.* 11 (2011) 175.
- (11) O. V. Dolomanov, L. J. Bourhis, R. J. Gildea, J. A. K. Howard, H. Puschmann, *J. Appl. Crystallogr.* 42 (2009) 339.
- (12) G. M. Sheldrick, *Acta Crystallogr. Sect. A: Found. Crystallogr.* 64 (2008) 112.

- (13)(a) L. Palatinus, G. Chapuis, *J. Appl. Crystallogr.* 40 (2007) 786; (b) L. Palatinus, A. van der Lee, *J. Appl. Crystallogr.* 41 (2008) 975; (c) L. Palatinus, S. J. Prathapa, S. van Smaalen, *J. Appl. Crystallogr.* 45 (2012) 575.
- (14) V. A. Blatov, A. P. Shevchenko, V. N. Serezhkin, *J. Appl. Crystallogr.* 33 (2000) 1193.
- (15) Y. Q. Sun, J. Zhang, Y. M. Chen, G. Y. Yang, *Angew. Chem. Int. Ed.* 44 (2005) 5814.
- (16) X. L. Wang, C. Qin, S. X. Wu, K. Z. Shao, Y. Q. Lan, S. Wang, D. X. Zhu, Z. M. Su, E. B. Wang, *Angew. Chem. Int. Ed.* 48 (2009) 5291.
- (17) M. Eddaoudi, J. Kim, N. Rosi, D. Vodak, J. Wachter, M. O'Keeffe, O. M. Yaghi, *Science* 295 (2002) 469.
- (18) D. R. Xiao, Y. G. Li, E. B. Wang, L. L. Fan, H. Y. An, Z. M. Su, L. Xu, *Inorg. Chem.* 46 (2007) 4158.
- (19) S. Y. Moon, E. Kim, T. H. Noh, Y. A. Lee, O. S. Jung, *Dalton Trans.* 42 (2013) 13974.
- (20) G. P. Yang, L. Hou, X. J. Luan, B. A. Wu, Y. Y. Wang, *Chem. Soc. Rev.* 41 (2012) 6992.
- (21)(a) J. Yang, Q. Yue, G. D. Li, J. J. Cao, G. H. Li, J. S. Chen, *Inorg. Chem.* 45 (2006) 2857; (b) X. J. Zheng, L. P. Jin, S. Gao, S. Z. Lu, *New J. Chem.* 29 (2005) 798; (c) W. Q. Kan, Y. Y. Liu, J. Yang, Y. Y. Liu, J. F. Ma, *CrystEngComm* 13 (2011) 4256; (d) X. L. Wang, C. Qin, E. B. Wang, Y. G. Li, N. Hao, C. W. Hu, L. Xu, *Inorg. Chem.* 43 (2004) 1850.

(22)(a) J. H. He, H. Y. Chen, D. R. Xiao, D. Z. Sun, G. J. Zhang, S. W. Yan, G. H.

Xin, R. Yuan, E. B. Wang, *CrystEngComm* 13 (2011) 4841; (b) G. L. Wen, Y. Y.

Wang, P. Liu, C. Y. Guo, W. H. Zhang, Q. Z. Shi, *Inorg. Chim. Acta* 362 (2009)

1730.

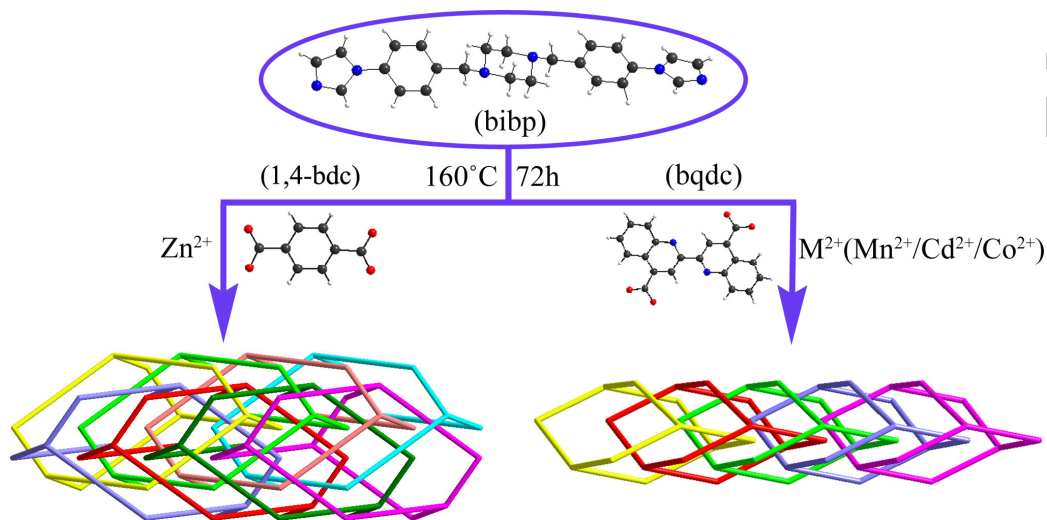
(23)(a) H. Y. Chen, D. R. Xiao, J. H. He, Z. F. Li, G. J. Zhang, D. Z. Sun, R. Yuan, E.

B. Wang, Q. L. Luo, *CrystEngComm* 13 (2011) 4988; (b) M. Kurmoo, *Chem.*

Soc. Rev. 38 (2009) 1353.

ACCEPTED MANUSCRIPT

Graphical Abstract - pictogram



ACCEPTED MANUSCRIPT

Graphical abstract - synopsis

Four novel coordination frameworks with high degree of diamondoid
interpenetration containing scarce quadruple-stranded homo-axis
helices and quintuple-stranded molecular braids

Yu Chen, Xi-Chi Wang, Qi-Yang, Yu-Ci Xu, Jin-Tao Tong, Hao Yuan and Dong-Rong

Xiao*

Four novel interpenetrated diamondoid (**dia**) networks obtained by self-assembly of a new long linear N-donor ligand and transition metal salts in the presence of short ditopic carboxylate ligands, provide an 8-fold [4+4] interpenetrated **dia** network containing the unique quadruple-stranded braid as well as an unprecedented octuple-stranded braid, and three 5-fold interpenetrating **dia** networks containing an exceptional quintuple-stranded molecular braid.

Highlights

Four novel coordination frameworks with high degree of diamondoid interpenetration containing scarce quadruple-stranded homo-axis helices and quintuple-stranded molecular braids

- (1) Compound **1** is an 8-fold [4+4] interpenetrated **dia** network.
- (2) Compound **1** contains unique quadruple-stranded intertwined homo-axis helices.
- (3) Compound **1** contains an inextricable octuple-stranded braid.
- (4) Compounds **2-4** display 5-fold interpenetrated **dia** networks.
- (5) Compounds **2-4** incorporate exceptional quintuple-stranded molecular braid.